

Fast Vibrational Modes and Slow Heterogeneous Dynamics in Polymers and Viscous Liquids

Francesco Puosi¹ , Antonio Tripodo¹ and Dino Leporini^{1,2,*} 

¹ Dipartimento di Fisica “Enrico Fermi”, Università di Pisa, Largo B. Pontecorvo 3, I-56127 Pisa, Italy; francesco.puosi@df.unipi.it (F.P.); antonio.tripodo@df.unipi.it (A.T.)

² Istituto per i Processi Chimico-Fisici-Consiglio Nazionale delle Ricerche (IPCF-CNR), via G. Moruzzi 1, I-56124 Pisa, Italy

* Correspondence: dino.leporini@unipi.it; Tel.: +39-050-2214937

Received: 25 October 2019; Accepted: 08 November 2019; Published: date

Abstract: Many systems, including polymers and molecular liquids, when adequately cooled and/or compressed, solidify into a disordered solid, i.e., a glass. The transition is not abrupt, featuring progressive decrease of the microscopic mobility and huge slowing down of the relaxation. A distinctive aspect of glass-forming materials is the microscopic dynamical heterogeneity (DH), i.e., the presence of regions with almost immobile particles coexisting with others where highly mobile ones are located. Following the first compelling evidence of a strong correlation between vibrational dynamics and ultraslow relaxation, we posed the question if the vibrational dynamics encodes predictive information on DH. Here, we review our results, drawn from molecular-dynamics numerical simulation of polymeric and molecular glass-formers, with a special focus on both the breakdown of the Stokes–Einstein relation between diffusion and viscosity, and the size of the regions with correlated displacements.

Keywords: glass transition; dynamical heterogeneity; Debye–Waller factor; diffusion; Stokes–Einstein relation

1. Introduction

When polymers, liquids, biomaterials, metals and molten salts are cooled or compressed, if the crystallization is avoided, they freeze into a microscopically disordered solid-like state, a glass [1–3]. On approaching the glass transition from states with high fluidity, the viscosity exhibits a huge increase of more than 10 orders of magnitude [1,2], along with the parallel decrease of the diffusivity [3,4]. Correspondingly, at microscopic level, solid-like behaviour becomes apparent, e.g., it is observed that a particle spends increasing time within the cage formed by the first neighbours where it rattles with amplitude $\langle u^2 \rangle^{1/2}$ on picosecond time scales [5]. This temporary trapping is rather persistent and the particle has average escape time, the structural relaxation time τ_α , which increases from a few picoseconds in the low-viscosity liquid up to thousands of seconds close to the glass transition [6]. The quantity $\langle u^2 \rangle$ appears in the expression of the Debye–Waller (DW) factor, which, assuming harmonicity and isotropy of the thermal motion, takes the form $\exp(-q^2 \langle u^2 \rangle / 3)$, where q is the absolute value of the scattering vector [7]. Researchers investigating the cage motion in viscous liquids usually refer, as a metonym, to $\langle u^2 \rangle$ as the DW factor too, e.g., see the work in [8–10]. To keep maintain similarity with this literature, the same convention is adopted here.

The transition from a liquid to a glass is accompanied by the growth of transient domains which exhibit different mobility, e.g., see Figure 1. The phenomenon is usually dubbed “dynamical heterogeneity” (DH) and has been extensively studied, e.g., see the reviews in [4,6,11,12] and topical papers [13–16]. The size of the domains is relatively small involving approximately 10 molecule diameters [11], corresponding to a few nanometres [14]. On a more general ground, the size of DH domains is strictly related to the possible presence of characteristic length scales in glass-forming systems. Starting with the seminal

paper by Adam and Gibbs, who invoked the presence of “cooperatively rearranging regions” in viscous liquids [17], increasing interest has been devoted to identifying possible growing length scales as mobility decreases [18,19]. A broad classification in terms of either static or dynamic length scales is usually used. Static (thermodynamic) length scales are determined by the free-energy landscape, whereas dynamic length scales are set by the rules governing the time evolution of the system and extracted from finite-time behaviour of time-dependent correlation functions and associated susceptibilities [6]. Even if growing static length scales have been reported by experiments [20] and simulations [21], there is still debate if they control the glass transition [22]. It is still not clear to what extent dynamic correlations are the consequence, or the primary origin of, slow dynamics occurring close to the glass transition [19].

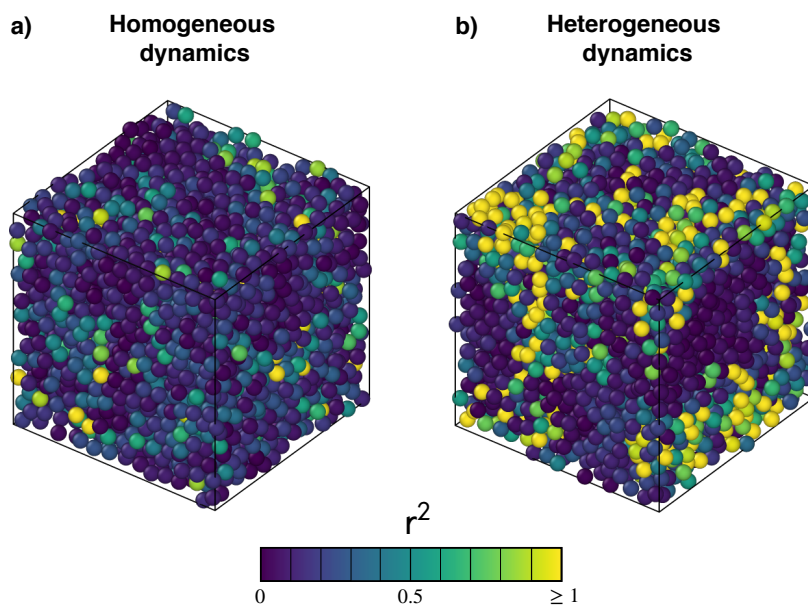


Figure 1. Monomer arrangements at a time t_0 of two states of a polymer melt with (a) homogeneous and (b) heterogeneous dynamics. Bonds are removed for clarity reasons. Particles are coloured according to their squared displacements in the time interval $[t_0 - \tau_\alpha, t_0]$. Bright yellow particles have squared displacements no less than 1. Notice that the two states have comparable mean square displacement (~ 0.21 , homogeneous state; ~ 0.28 , heterogeneous state) but rather different relaxation times τ_α (~ 9 , homogeneous state; ~ 1550 , heterogeneous state). Homogeneous, i.e., position-independent, dynamics of the monomers is an aspect of systems with fast relaxation. Conversely, in the presence of heterogeneous dynamics, clusters of particles with extremely high mobility coexist with nearly immobile ones, slowing down the relaxation.

Even if rooted at nanometric length scales, DH exerts clear influence at macroscopic level. One widely studied phenomenon is the breakdown of the Stokes–Einstein (SE) relation involving the diffusion coefficient D and the shear viscosity η (the more debated analogous phenomenon involving the rotational diffusion, where the breakdown is revealed [23,24] or missing [11], will not be considered here). For a single particle with radius R moving in a homogeneous fluid with viscosity η at temperature T , the SE relation states that

$$D = \frac{k_B T}{\zeta \pi \eta R} \quad (1)$$

k_B denotes the Boltzmann constant and ζ denotes a number depending on the boundary condition between the fluid and the particle [25]. Under a no-slip condition, $\zeta = 6$. Roughly, the SE law states that the quantity $k_B T / D \eta$ is a constant of the order of the size of the diffusing particle. Remarkably, despite its macroscopic derivation, SE also well accounts for the self-diffusion of many monoatomic and molecular liquids, provided the viscosity is low ($\lesssim 10$ Pa · s) [26]. On the other hand, the finite diffusion coefficient of guest atoms in solid hosts, where viscous transport is missing strongly, suggest the SE failure close to the solidification occurring at the glass transition. In fact, a common feature of several fragile glass formers is the SE breakdown for increasing viscosity. The failure manifests itself as a partial decoupling between the diffusion and the viscosity, in the sense that D^{-1} increases less than η [4,11,27–30]. The decoupling is well accounted for by the fractional SE $D \sim \eta^{-\kappa}$ [31], where the non-universal exponent κ falls in the range $0.5 \leq \kappa < 1$ [15]. The usual interpretation of the SE breakdown relies on DH and the subsequent presence of a spatial distribution of characteristic relaxation times τ close to the glass transition [6,11,31]. The neat argument is that, although the viscosity is more sensitive to the longest relaxation times, the diffusivity is influenced by the shortest ones. As the shape of the distribution tends to widen on approaching the glass transition, the gap between D^{-1} and η increases as well, leading to the SE breakdown [4].

Diffusion, viscous transport, and structural relaxation involve time scales that are much longer than the typical vibrational time t^* of the particle rattling in the cage of the first neighbours, typically a few picoseconds. The diffusion coefficient is expressed as $D = 6\delta^2 / \tau_D$, where τ_D is the minimum time ensuring that the particle random displacements at a pace τ_D are statistically independent with finite mean square value δ^2 [25]. On the other hand, the viscous flow requires the relaxation of the shear stress fluctuation, which occurs in a Maxwell time $\tau_M = \eta / G$, where G is the intermediate-time shear modulus [32]. On approaching the glass transition, $t^* \ll \tau_D, \tau_M, \tau_\alpha$.

Despite the huge difference in time scales, earlier [33] and later theoretical studies [5,34–40], and experimental ones [41], addressed the rattling process within the cage to understand the slow dynamics, rising a growing interest on the DW factor [8,29,30,42–61]. Within this context, most interest has been devoted to the correlations between DW factor and the structural relaxation time τ_α , which are found to be strong and encompassed by a universal master curve [47]:

$$\tau_\alpha = \mathcal{F}(\langle u^2 \rangle) \quad (2)$$

An analytical expression of the master curve is derived in Section 2. Alternative forms of the master curve are reported by Douglas and coworkers [8–10]. Correlations between DW factor and the structural relaxation time τ_α are found in polymers in bulk [30,47–49] and thin films [61], binary atomic mixtures [48, 55], colloidal gels [52], antiplasticised polymers [8,9], water [57] and water-like models [59,60]. The DW factor also provided an alternative interpretation of the so-called thermodynamic (or temperature/density) scaling [58]. The correlation between structural relaxation and DW factor has been inspected in the experimental data concerning several glass-formers in a wide range of fragility—the steepness index m defined by Angell [1] ($20 \leq m \leq 191$), including polymers, van der Waals and hydrogen-bonded liquids, metallic glasses, molten salts and the strongest inorganic glass-formers [47,50,51,55–58].

The structural relaxation time τ_α is an average quantity which is certainly affected by DH but not in a straightforward way. Nonetheless, given the scaling expressed by Equation (2), it is legitimate to wonder if DH and fast vibrational dynamics exhibit correlations. Working in that direction, we have found positive answers and the present paper collects and reviews a selected part of our results, with a focus on the breakdown of the SE law [29,30]. Even if strictly related, we will not discuss here a study concerning ultrathin molecular films with strong mobility gradients analogous to DH, where the same scaling observed in bulk, Equation (2), has been revealed [61].

Our approach relies on the increasing evidence that the master curve, Equation (2), is a manifestation of a more fundamental correlation between the vibrational dynamics and the slow relaxation. It may be presented in the following terms. Let us consider a generic space- and time-dependent correlation function $C(\mathbf{x}_1, t_1; \mathbf{x}_2, t_2)$, where \mathbf{x} denotes a configuration of the liquid at a given time t , i.e., the set \mathbf{x} of all the positions of the elementary microscopic particles (monomers, atoms, molecules, etc.). For steady states, $C(\mathbf{x}_1, t_1; \mathbf{x}_2, t_2)$ depends on the time difference $t = t_2 - t_1$. Let us set $t_1 = 0$ and define $C(\mathbf{x}_0; \mathbf{x}, t) \equiv C(\mathbf{x}_0, 0; \mathbf{x}, t)$. If two states, labelled by a and b , have equal DW factor, the correlation function, when evaluated over the two states, has coincident time evolution at least between the typical vibrational time scale t^* and τ_α [49]. Said otherwise, for $t^* \lesssim t \lesssim \tau_\alpha$, it holds [32,47,49–51,53–55]:

$$\langle u^2 \rangle_{(a)} = \langle u^2 \rangle_{(b)} \Rightarrow C(\mathbf{x}_0; \mathbf{x}, t)_{(a)} = C(\mathbf{x}_0; \mathbf{x}, t)_{(b)} \quad (3)$$

In selected systems, Equation (3) holds beyond τ_α and extends up to the diffusive regime, e.g., unentangled polymers and atomic binary mixtures [29,30,49,55].

Our studies were prompted by the finding by Widmer-Cooper and Harrowell that DH are predicted by particle displacements at short times [44]. However, it must be stressed that our DW factor is evaluated within the vibrational time scale t^* and not the time scale in [44], which is approximately one order of magnitude longer, a choice leading to differences for states with low viscosity.

The review outlines a model of the slow heterogeneous relaxation and transport in terms of vibrational dynamics in Section 2. The model is presented for completeness, but it is not essential to the understanding of the simulation results discussed in the rest of the paper. Later, a broad introduction to relaxation and transport in polymeric melts, and the correlation with the vibrational fast dynamics is given in Sections 3 and 4, respectively. The signatures identifying the presence of heterogeneous dynamics are discussed in Section 5. The SE breakdown is presented in Section 6, with a final discussion on the length scale of the mutual influence between particle displacements in Section 7.

2. A model of the Slow Heterogeneous Relaxation and Transport in Terms of Vibrational Dynamics

An in-depth, microscopic understanding of the link between the fast and slow dynamics is still missing, even if the impact of anharmonicity has been noted [43,58,62]. Here, we present a model, extending first seminal ideas [34], where the key role is played by the DW factor $\langle u^2 \rangle$, which is a single-particle quantity. Alternative pictures, in terms of the same quantity, are known [8–10]. Notice that, even if a single-particle quantity, the DW factor encodes information on collective dynamics and spatially extended cooperative phenomena [32,53,54,62–64].

At the present level of development, the model delivers expressions of the diffusion coefficient and the structural relaxation time in terms of the DW factor. It also accounts for the nonexponential character of the relaxation, an aspect which will be not presented here. However, even if it incorporates some consequence of DH, i.e., the presence of a wide distribution of relaxation times $p(\tau)$, it does not cover any spatial aspect related to DH, which instead has been revealed by the simulations, as we will see in Sections 5.1 and 7, and accounted for by Equation (3).

2.1. Relaxation Time

A first basis to connect fast and slow degrees of freedom was developed by Hall and Wolynes who, assuming that atomic motion is restricted to cells, pictured the glass transition as a freezing in an aperiodic crystal structure [34]. As a result, the viscous flow is described in terms of activated jumps over energy

barriers $\Delta E \propto k_B T a^2 / \langle u^2 \rangle$, where a is the displacement to reach the transition state. The usual rate theory leads to the Hall–Wolynes equation:

$$\tau_\alpha^{(HW)}(a^2), \eta^{(HW)}(a^2) \propto \exp\left(\frac{a^2}{2\langle u^2 \rangle}\right) \quad (4)$$

Equation (4) has the form of Equation (2). A very similar relation was derived by Buchenau and Zorn, in terms of soft vibrational modes [41]. Equation (4) is expected to fail when τ_α becomes comparable to the typical rattling times of each atom in the cage, corresponding to picosecond timescales. This condition is quite mild, e.g., in selenium it occurs ~ 100 K above the melting temperature [41].

One basic assumption of Equation (4) is that the distance to reach the transition state has a characteristic value a . Actually, this length scale is dispersed. To constrain the related distribution, $p(a^2)$, it is assumed that the latter does not depend on the state parameters such as the temperature, the density or the interacting potential. This complies with the spirit of the work in [34], where the a distance is said to be mostly controlled by the geometrical packings. It is also known that, irrespective of the relaxation time, τ_α , the average distance moved by the relaxing unit within τ_α is approximately the same, i.e., a fraction of the molecular diameter [1]. Averaging Equation (4) over the distribution $p(a^2)$ yields the structural relaxation time

$$\tau_\alpha = \left\langle \tau_\alpha^{(HW)}(a^2) \right\rangle_{a^2} \quad (5)$$

$$\equiv \int_0^\infty \tau_\alpha^{(HW)}(a^2) p(a^2) da^2 \quad (6)$$

Note that Equation (6) assumes that the distribution of the relaxation times is mainly due to the distribution of the displacement to reach the transition state in the different local environments, whereas the average DW factor $\langle u^2 \rangle$ is taken as homogeneous across the sample. This viewpoint relies on the picture that relaxation is related to long wavelength soft modes [41,46]. Support has been provided by the strong correlation observed in glass-formers between $\langle u^2 \rangle$ and the elastic modulus under quasi-static mechanical equilibrium [32].

As a suitable choice, the distribution of the squared distances $p(a^2)$ is taken as a truncated Gaussian form [47,48]

$$p(a^2) = \begin{cases} A \exp\left(-\frac{(a^2 - \bar{a}^2)^2}{2\sigma_{a^2}^2}\right) & \text{if } a > a_{min} \\ 0 & \text{otherwise} \end{cases} \quad (7)$$

where A is the normalization ensuring $\int_0^\infty p(a^2) da^2 = 1$ and a_{min}^2 is the minimum displacement to reach the transition state. Given the weak influence, and to get rid of an adjustable parameter, one takes $a_{min}^2 = 0$ [47,48]. The motivations behind the Gaussian form of $p(a^2)$ mainly rely on the Central Limit Theorem. In fact, a^2 (r_0^2 in the notation in [34]) is the cumulative squared displacement of the N_{mon} particle that move [34].

Plugging Equation (7) into Equation (6) leads to the following generalized HW equation (GHW),

$$\tau_\alpha = \tau_0 \exp\left(\frac{\bar{a}^2}{2\langle u^2 \rangle} + \frac{\sigma_{a^2}^2}{8\langle u^2 \rangle^2}\right) \quad (8)$$

τ_0 is a suitable constant. An analogous law is anticipated for the viscosity η , given the known near proportionality with τ_α [3]. Equation (8) is the form of the master curve Equation (2) being adopted in our

studies. Other variants useful in the comparison with numerical and experimental results are listed in Appendix A and B.

Obviously, if the distribution $p(a^2)$ is narrow and centred at a_0^2 , Equation (8) must reduce to the expression derived by Hall and Wolynes, Equation (4), $\tau_\alpha^{(HW)}(a_0^2)$. For the specific choice of $p(a^2)$, given by Equation (10), Equation (8) shows that this happens if $\sigma_{a^2}^2/8\langle u^2 \rangle^2 \ll \bar{a}^2/2\langle u^2 \rangle$, namely, the ratio R defined as

$$R \equiv \sigma_{a^2}^2/4\bar{a}^2\langle u^2 \rangle \quad (9)$$

is vanishingly small. Equation (9) depends on the magnitude of DW factor so that, being the parameters $\sigma_{a^2}^2$ and \bar{a}^2 independent of the physical state, the presence of the distribution $p(a^2)$ is negligible when the DW factor is large, thus leading to a very narrow distribution of relaxation times, a characteristic of homogeneous dynamics. This suggests to read the condition $R = 1$ as the crossover between homogeneous and heterogeneous dynamics, i.e.,

$$\begin{cases} R \ll 1 & \text{homogeneous dynamics} \\ R \gg 1 & \text{heterogeneous dynamics} \end{cases} \quad (10)$$

Finally, we notice that the distribution $p(a^2)$ in Equation (7) with $a_{min}^2 = 0$ may be recast via Equation (4), as a log-normal distribution of relaxation times $p(\ln \tau)$

$$p(\ln \tau) = \begin{cases} B \exp \left\{ -\frac{2\langle u^2 \rangle^2}{\sigma_{a^2}^2} \left[\ln \left(\frac{\tau}{\bar{\tau}} \right) \right]^2 \right\} & \text{if } \tau \geq \tau_0 \\ 0 & \text{otherwise} \end{cases} \quad (11)$$

where B is the normalization ensuring $\int p(\ln \tau) d \ln \tau = 1$, $\bar{\tau} = \tau_0 \exp(\bar{a}^2/2\langle u^2 \rangle)$. An interesting feature of $p(\ln \tau)$ is that its width $\sim \sigma_{a^2}/\langle u^2 \rangle$ increases by decreasing the DW factor.

2.2. Diffusion Coefficient

The diffusion coefficient D may be expressed via the above model by the relation [30]

$$D = \frac{1}{6} \left\langle \frac{a^2}{\tau_\alpha^{(HW)}(a^2)} \right\rangle_{a^2} \quad (12)$$

The above equation assumes that displacements as large as a occurring in a time $\tau_\alpha^{(HW)}(a^2)$ are statistically independent. Notice that, although Equation (6) signals that the structural relaxation time is affected by the larger a^2 values, i.e., the longest relaxation times of the distribution $p(\ln \tau)$, the diffusivity, according to Equation (12), is influenced by the shorter ones.

The explicit expression of the diffusion coefficient and an approximated version are given in Appendix A.2.

2.3. Stokes–Einstein Product

The Stokes–Einstein (SE) relation, Equation (1), states that the quantity $D\eta/T$ is constant if the diffusing particle changes neither the size nor the boundary conditions with the liquid. As the numerical evaluation of the viscosity is a delicate point, proxies are often used [27,65]. As an example, as $\eta \propto T\tau_\alpha$ in

unentangled polymers [66], it is more suitable to study the breakdown of the SE law by considering the SE product

$$K_{SE} = DM\tau_\alpha \quad (13)$$

where M is the number of monomers. K_{SE} is expected to be independent of the chain length, as $D \propto 1/M$ in unentangled polymers [66] and the monomer relaxation at τ_α poorly senses the chain connectivity. The above equation with $M = 1$ may be also used for liquids where the elementary units are atoms or small molecules, as the temperature factor in the ratio $D\eta/T$ provides a change of approximately $\sim 20\%$ in fragile glass-formers [3], much less than the observed increase of K_{SE} on approaching the glass transition [4,11]. The explicit expression of the SE product K_{SE} derived within the vibrational dynamics model and an approximated version \tilde{K}_{SE} are given in Appendix A.3.

3. Transport and Relaxation in Polymeric Melts

The correlation between diffusivity, slow relaxation and fast vibrational dynamics has been studied by Molecular-Dynamics (MD) simulations of a coarse-grained model of a melt of linear unentangled polymer. Details about the model are given in Section 9. Even if rather crude, the model was proven to capture the universal aspects of the correlation and allowed an effective comparison with the experiment [47].

To provide a microscopic picture of the transport, the mean square displacement (MSD) of the monomer $\langle r^2(t) \rangle$ is usually considered:

$$\langle r^2(t) \rangle = \frac{1}{N} \sum_i \langle \|\mathbf{x}_i(t) - \mathbf{x}_i(0)\|^2 \rangle \quad (14)$$

where $\mathbf{x}_i(t)$ is the position of the i -th monomer at time t . In addition to MSD, with the purpose of characterizing the relaxation, the self part of the intermediate scattering function (ISF) is also considered [26]:

$$F_s(q, t) = \frac{1}{N} \left\langle \sum_j e^{i\mathbf{q} \cdot (\mathbf{x}_j(t) - \mathbf{x}_j(0))} \right\rangle \quad (15)$$

In an isotropic liquid, ISF depends only on the modulus of the wavevector $q = \|\mathbf{q}\|$ and features the rearrangements of the spatial structure of the fluid over the length scale $\sim 2\pi/q$, leading to a decaying profile in time starting from $F_s(q, 0) = 1$. In our case, ISF was evaluated at $q = q_{max}$, the maximum of the static structure factor ($7.13 \leq q_{max} \leq 7.55$) corresponding to the length scale of the monomer size. $F_s(q_{max}, t)$ vanishes when the monomer displacement in a time t largely exceeds the monomer diameter. The time needed to make $F_s(q_{max}, t)$ small is a measure of the escape time of the monomer from the cage formed by the neighbours, also known as the structural relaxation time τ_α , customarily defined by the relation $F_s(q_{max}, \tau_\alpha) = e^{-1}$.

Figure 2 shows typical MSD and ISF curves of the polymeric monomers. At very short times (ballistic regime), MSD increases according to $\langle r^2(t) \rangle \cong (3k_B T/m)t^2$ and ISF starts to decay. The repeated collisions with the other monomers slow the displacement of the tagged one, as evinced by the knee of MSD at $t \sim \sqrt{12}/\Omega_0 \sim 0.17$, where Ω_0 is an effective collision frequency, i.e., it is the mean small oscillation frequency of the monomer in the potential well produced by the surrounding ones kept at their equilibrium positions [64,67]. At later times, a quasi-plateau region, also found in ISF, occurs when the temperature is lowered and/or the density increased. This signals the increased caging of the particle. Trapping is terminated after an average time τ_α . For $t \gtrsim \tau_\alpha$, MSD increases more steeply. The monomers of short chains ($M \lesssim 3$) undergo diffusive motion $\langle r^2(t) \rangle \propto t^\delta$ with $\delta = 1$. For longer chains, owing to the increased connectivity, the onset of the diffusion is preceded by a subdiffusive region ($\delta < 1$, Rouse regime) [68]. At long time, the monomer displaces in a diffusive way with diffusion coefficient $D = \lim_{t \rightarrow \infty} \langle r^2(t) \rangle / 6t$.

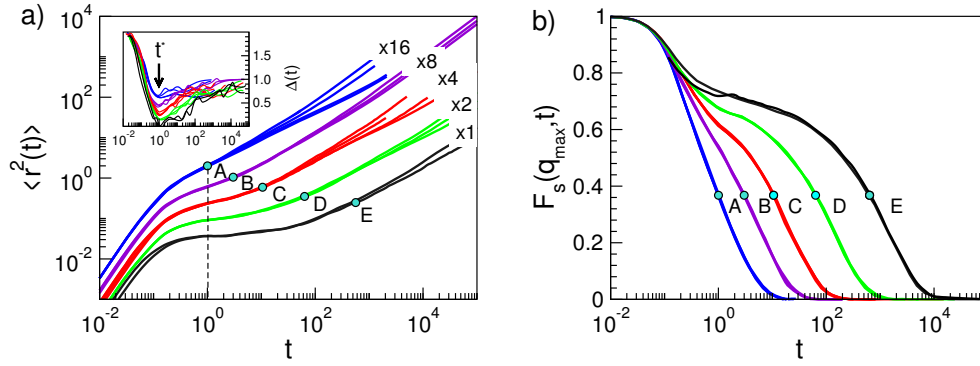


Figure 2. Monomer dynamics in the polymer melt. (a) Mean square displacement (MSD) for polymers in selected states (see below for details). For clarity reasons, MSDs are multiplied by indicated factors. Inset: corresponding MSD slope $\Delta(t)$, Equation (16); the position of the minimum at $t^* = 1.0(4)$ is signalled by the arrow in the inset and the dashed line in the main panel. (b) corresponding ISF curves. The figure shows a manifestation of Equation (3), see Section 5.1 for details, i.e., if states have equal DW factor $\langle u^2 \rangle$, both the MSD and ISF curves coincide at least in the time window $[t^*, \tau_\alpha]$ (τ_α is marked with dots on each curve). The physical states are labelled by the string (M, ρ, T, q, p) where M is the number of monomers per chain, ρ the number density, T the temperature and the pair (q, p) refers to the characteristic parameters of the non-bonding potential, Equation (25). The six sets of states are as follows. Set A: (2,1.086,0.7,7,6), (3,1.086,0.7,7,6), (10,1.086,0.7,7,6), (10,1.033,0.7,8,6). Set B: (2,1.033,0.7,10,6), (3,1.039,0.7,11,6), (3,1.041,0.7,11,6). Set C: (2,1.033,0.5,10,6), (3,1.056,0.7,12,6), (5,1.033,0.6,12,6), (10,1.056,0.7,12,6). Set D: (3,1.086,0.7,12,6), (5,1.086,0.7,12,6), (10,1.086,0.7,12,6). Set E: (2,1.0,0.7,12,11), (3,1.1,1.1,15,7). Data from [48].

4. Correlation between Vibrational Fast Dynamics and Slow Relaxation

4.1. Vibrational Caged Dynamics and Debye–Waller factor

In our model polymer, the term “vibrational dynamics” refers to the rattling of the trapped monomer within the cage formed by the closest monomers. It is crucial to provide a robust criterion to assess the presence of the cage, which is anticipated to lack in liquids with high molecular mobility and fast relaxation. Compelling evidence of the cage effect is provided by the time velocity correlation function, which, after a first large drop due to pair collisions, reverses the sign since the monomer rebounds from the cage wall [64]. As an alternative route to reveal the cage effect, we consider the slope of MSD in the log-log plot

$$\Delta(t) \equiv \frac{\partial \log \langle r^2(t) \rangle}{\partial \log t} \quad (16)$$

Representative plots of $\Delta(t)$ for the polymer system are given in the inset of Figure 2a. $\Delta(t)$ tends to 2 at short times, due to the ballistic motion, and reaches the plateau level 1 at long times, owing to the diffusive motion. In the absence of caging effect, $\Delta(t)$ decreases in a monotonous way on increasing time. Caging is indicated by the presence of a minimum of $\Delta(t)$ occurring, irrespective of the physical state in the present model polymer, at $t^* = 1.0(4)$. In actual time units, t^* is ~ 1 – 10 ps [69].

The presence of the minimum paves the way to a robust definition of the DW factor $\langle u^2 \rangle$, the mean square rattling amplitude of the monomer during the trapping period. In fact, the minimum, corresponding to the inflection point in the log-log plot of $\langle r^2(t) \rangle$, separates two regimes. At short times, $t < t^*$, the inertial effects dominate, whereas for $t > t^*$, early escapes from the cage become apparent. Therefore, a convenient definition of the DW factor as a mean localization length is just MSD at t^* :

$$\langle u^2 \rangle \equiv \langle r^2(t = t^*) \rangle \quad (17)$$

4.2. Debye–Waller Scaling of the Slow Relaxation

The monomer dynamics depends in a complex way on the state parameters. Nonetheless, there is clear correlation between the DW factors and the long-time relaxation dynamics. First examples are shown in Figure 2 by considering MSD and ISF. Note that states with equal DW factor have coincident time evolution of both MSD and ISF at least between t^* and τ_α [49]. In Section 5.1, it will be shown that these results are a manifestation of Equation (3).

It is seen that the coincidence of the MSD curves is lacking at times longer than τ_α for states corresponding to polymer chains with different length. This effect is not a failure of the scaling at times exceeding τ_α , but a mere consequence of the complex dependence of MSD on the chain length since it is affected by all the Rouse modes [66]. In fact, if the correlation function of the single Rouse mode with the slowest relaxation time is singled out, i.e., the one with characteristic relaxation time given by the average chain reorientation time τ_{ee} [66], the scaling is still observed after proper account of the chain length dependence, see Figure 3. The finding proves that Equation (3) holds also at a time τ_{ee} being much longer than τ_α .

As a side product of the coincidence of the ISF curves in states with equal DW factor seen in Figure 2, one has that states with equal DW factor $\langle u^2 \rangle$ have equal structural relaxation time τ_α too. This can be reformulated via the master curve Equation (2), which, according to the model detailed in Section 2.1, takes the form given by Equation (8), i.e., a simple parabolic law between $\log \tau_\alpha$ and $1/\langle u^2 \rangle$ [47,48]. Figure 4 tests Equation (8), written in the form given by Equation (A1) for a wide variety of physical states of our model polymeric melt [48]. It is also shown that the scaling holds if one considers the end–end chain reorientation time τ_{ee} , i.e., the time needed by the correlation function $C_{ee}(t)$ to drop to e^{-1} , see Figure 3; although, in this case, it is described by a different master curve.

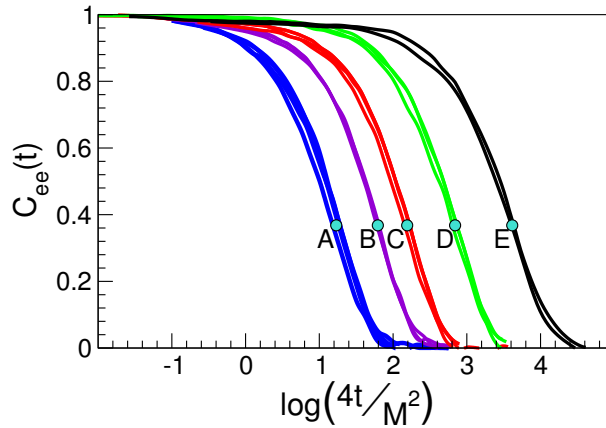


Figure 3. Correlation function of the end-to-end vector joining the two ends of a polymer chain. Each group of curves corresponds the physical states A, . . . , E with identical DW factor detailed in Figure 2. Polymer states contributing to one cluster of scaled curves have not necessarily equal chain length. However, the scaled time removes the chain length dependence. Dots mark the time $4\tau_{ee}/M^2$. The results prove that Equation (3) holds also at times τ_{ee} much longer than τ_α . Data from [48].

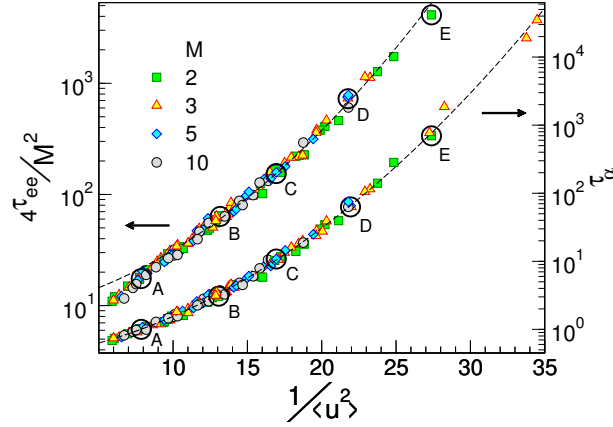


Figure 4. The structural relaxation time τ_{α} and the scaled reorientation time τ_{ee} of the polymer chains vs. the DW factor $\langle u^2 \rangle$. Empty circles highlight the cases plotted in Figure 2. The other states are detailed in Ref. [48]. The dashed line across the τ_{α} curve is Equation (A1). The dashed curve across the chain reorientation time curve is a guide for the eyes. Data from [48].

5. Signatures of the Heterogeneous Dynamics

MSD and ISF well-expose the cage effect, whereas the possible DH influence on their shape is less apparent. Figure 1 shows that DH is characterized by the presence of clusters of monomers with rather different mobility [11,12]. We now present and discuss two quantities well tailored to provide quantitative insight into this aspect.

5.1. van Hove Function

One central quantity of the DH analysis is the self part of the van Hove function $G_s(\mathbf{r}, t)$ [26]:

$$G_s(\mathbf{r}, t) = \frac{1}{N} \left\langle \sum_{i=1}^N \delta[\mathbf{r} + \mathbf{x}_i(0) - \mathbf{x}_i(t)] \right\rangle \quad (18)$$

where $\mathbf{x}_i(t)$ is the position of the i -th monomer at time t , and $\delta[\cdot]$ is the three-dimensional Dirac delta function. In isotropic liquids, the van Hove function depends on the modulus r of \mathbf{r} . The interpretation of $G_s(r, t)$ is direct. The product $G_s(r, t) \cdot 4\pi r^2$ is the probability that the monomer is at a distance between r and $r + dr$ from the initial position after a time t . The moments of $G_s(r, t)$ are of interest:

$$\langle r^n(t) \rangle = 4\pi \int_0^{\infty} r^n G_s(r, t) r^2 dr \quad (19)$$

For $n = 2$, one recovers the usual mean square displacement (MSD). If the monomer displacement is a Gaussian random variable, $G_s(r, t)$ reduces to the Gaussian form [26]:

$$G_s^g(r, t) = \left(\frac{3}{2\pi \langle r^2(t) \rangle} \right)^{3/2} \exp \left(-\frac{3r^2}{2 \langle r^2(t) \rangle} \right) \quad (20)$$

Equation (20) is the correct limit of $G_s(r, t)$ at very short (ballistic regime, $\langle r^2(t) \rangle = 3k_B T / \mu t^2$) and very long times (diffusion regime, $\langle r^2(t) \rangle = 6Dt$, where D is the monomer diffusion coefficient).

The spatial Fourier transform of the self part of the van Hove function yields the ISF function, Equation (15) [26].

Figure 5a presents the self-part of the van Hove function $G_s(r, t)$, evaluated at τ_α for the set of states with different mobility and relaxation shown in Figure 2. It is seen that if the relaxation and the mobility are fast, the shape of $G_s(r, \tau_\alpha)$ decreases by increasing the displacement r from the initial position. On the other hand, the states belonging to the D and E set, the ones with slowest relaxation, exhibit a tendency toward a bimodal pattern, namely, in addition to particles undergoing small displacements, a shoulder at $r \sim 1$ (the monomer diameter) is observed. This signals the presence of particles exhibiting fast displacements by solid-state jump dynamics [27]. Said otherwise, the quasi-bimodal pattern of the van Hove function is clear signature of DH. Four other aspects are to be noted:

- The self-part of the van Hove function is expressed by suitable correlation functions, see Appendix B. Then, the coincidence of $G_s(r, \tau_\alpha)$ in states with equal DW factor observed in Figure 5a (the sets of states labelled as A, . . . , E) is in harmony with Equation (3).
- Equation (3) also holds if one inspects the spatial dependence of the correlation function, e.g., the van Hove function, at τ_α . In particular, even in the presence of DH.
- Given their relation with $G_s(r, t)$, the coincidence of both MSD and ISF observed in Figure 2 for the sets of states labelled as A, . . . , E is strictly linked to the one observed in Figure 5a.
- The pattern of the D and E sets of states is not consistent with the Gaussian limit $G_s^g(r, \tau_\alpha)$, Equation (20), predicting a progressive decay with r , i.e., the DH dynamics is *not* Gaussian;

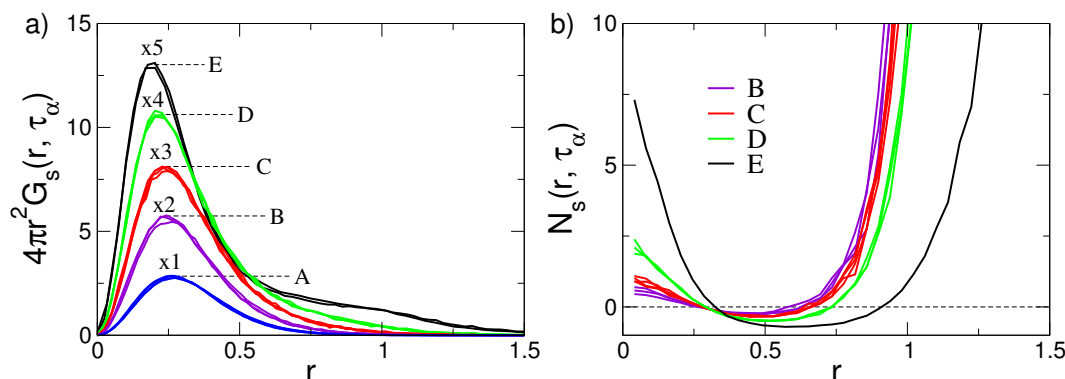


Figure 5. (a) Self part of the van Hove function $G_s(r, t)$ of the states of Figure 2 at the structural relaxation time $t = \tau_\alpha$. The curves are multiplied by indicated factors. The sets of clustered curves A–E show that, if states have equal DW factor, they have coincident van Hove functions too. As $G_s(r, t)$ may be expressed in terms of correlation functions, the coincidence reflects Equation (3). Data from [49]. (b) The ratio $N_s(r, \tau_\alpha)$, Equation (21), of the states of Figure 2. On increasing the structural relaxation time from A states to E states, the system tends to increase the fractions of monomers with either much lower or much higher mobility with respect to the fraction predicted by the Gaussian approximation. Data from [53].

To quantify the deviations of the self-part of the van Hove function $G_s(r, \tau_\alpha)$ from the Gaussian limit, one defines the quantity [27,70]

$$N_s(r, \tau_\alpha) = \frac{G_s(r, \tau_\alpha) - G_s^g(r, \tau_\alpha)}{G_s^g(r, \tau_\alpha)} \quad (21)$$

Figure 5b plots the ratio $N_s(r, \tau_\alpha)$. It exhibits increasing positive deviations at both short and large r values, evidencing the excess of nearly immobile and highly mobile monomers with respect to purely Gaussian behaviour, respectively. The analysis, in terms of the ratio $N_s(r, \tau_\alpha)$, reveals the wide distribution of mobilities pictured in Figure 1, right.

5.2. Non-Gaussian Parameter

An effective quantity to expose the time evolution of the non-Gaussian character of DH dynamics is the non-Gaussian parameter (NGP) [26]:

$$\alpha_2(t) = \frac{3}{5} \frac{\langle r^4(t) \rangle}{\langle r^2(t) \rangle^2} - 1 \quad (22)$$

where $\langle r^2(t) \rangle$ and $\langle r^4(t) \rangle$ are the mean square and quartic displacements of the particle at time t , respectively. α_2 vanishes if the displacement is Gaussian, i.e., it follows from a series of independent elementary steps with finite mean and variance.

Figure 6 plots the NGP time evolution, Equation (22), for the set of states A, \dots , E and additional states with very slow relaxation. It is seen that NGP vanishes at very short times, as the ballistic regime is Gaussian in nature. At intermediate times, a peak value α_2^{max} is observed increasing with the relaxation times [46,71,72]. The maximum occurs at a time slightly shorter than the structural relaxation time τ_α , as in simpler molecular systems [27]. A snapshot of the microscopic mobilities in a lapse of time τ_α , where DH is quite apparent, is plotted in Figure 1 (right). At later times, NGP decreases as the monomer dynamics enters the homogeneous diffusive regime, which is a Gaussian process [25].

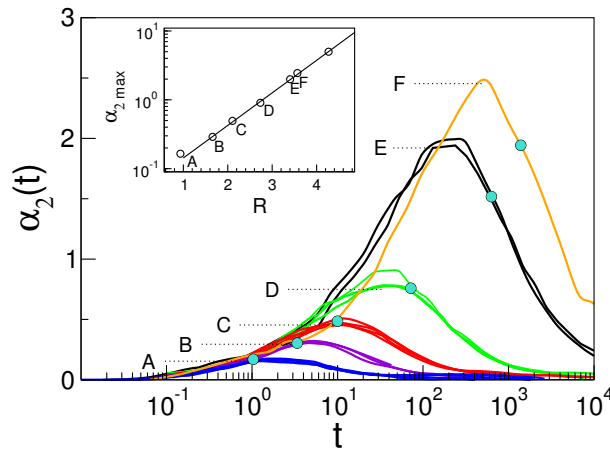


Figure 6. Non-Gaussian parameters (NGPs) of states with different relaxation times τ_α (marked with grey dots). The physical states A, \dots , E are the states with identical DW factor detailed in Figure 2. Note that they have coinciding NGPs in the time window $[t^*, \tau_\alpha]$ at least, in agreement with Equation (3). The curve labelled as F is the state $(M, \rho, T, q, p) = (3, 1.1, 0.65, 12, 6)$ with $\tau_\alpha \simeq 2 \cdot 10^3$, see Figure 4. Inset: the NGP maximum α_2^{max} vs. the ratio R , Equation (9). The dot with the largest α_2^{max} value corresponds to the state with the longest structural relaxation time τ_α in Figure 4 with parameters $(M, \rho, T, q, p) = (3, 1.2, 0.95, 6, 12)$. Data from [29].

It is seen that states belonging to the same set A, \dots , E, i.e., with equal DW factor, have identical NGP in the time window $[t^*, \tau_\alpha]$ at least. This agrees with Equation (3), given the relation of NGP with the moments of the self part of the van Hove function $G_s(r, t)$, Equation (19), and the expression of the latter in terms of suitable correlation functions, see Appendix B [73]. Note also the exponential increase of α_2^{max} with the ratio R defined in Equation (9) [47,48]. This is in harmony with the inequalities in Equation (10), stating that DH is characterized by $R > 1$.

6. Breakdown of the Stokes–Einstein (SE) Law in the Presence of Dynamical Heterogeneity

6.1. SE Breakdown in Unentangled Polymers

The SE law is usually derived by considering the diffusivity of macroscopic bodies displacing in homogeneous viscous liquids [25]. The diffusion in the presence of strong DH does not comply with the SE law [15]. We have studied the SE breakdown in melts of unentangled polymers [29]. In these systems, helpful features are found [66]: (i) the diffusion coefficient D is inversely proportional to the chain length M , and (ii) the viscosity η is proportional to the end–end reorientation time which, in turn, is proportional to the structural relaxation time, e.g., see Figure 3, showing that states with equal structural relaxation time also have equal end–end reorientation time. Then, as discussed in Section 2.3, the study of the validity of the SE law is more efficiently carried out in terms of the product $DM\tau_\alpha$, which is anticipated to be state-independent if the SE law holds.

Figure 7 shows that in states with homogeneous Gaussian dynamics, i.e., with small α_2^{\max} values, the R values are comparable or less than the unit value and the product $DM\tau_\alpha$ is nearly constant, i.e., the SE law holds true. On the other hand, in the presence of significant DH, i.e., $\alpha_2^{\max} > \alpha_{2,c}^{\max} = 0.40(5)$, one finds $R > R_c = 1.9(1)$ and the product $DM\tau_\alpha$ tends to increase, i.e., the SE law fails [11,12,27]. The comparison between α_2^{\max} and R substantiates the conclusion that the magnitude of the ratio R allows one to conclude whether DH is appreciable or not, as suggested by Equation (10). As the ratio R —apart from constants—depends only on DW, see Equation (9), the finding supports previous conclusions that the long-time DH is rooted in the fast dynamics [44].

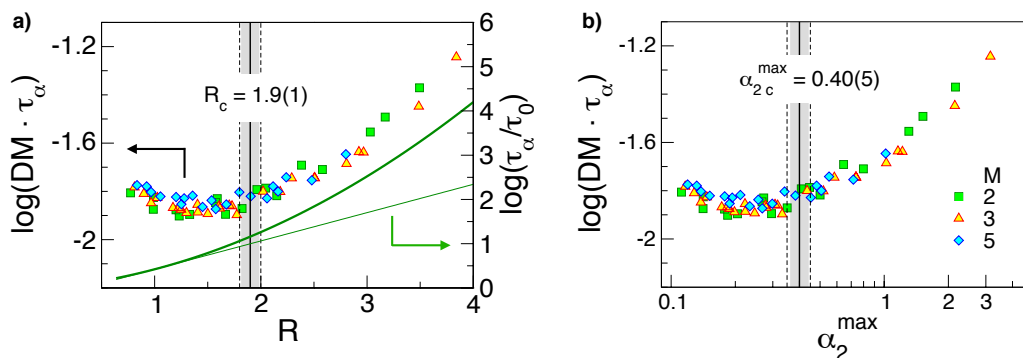


Figure 7. (a) The product $DM\tau_\alpha$ vs. the ratio R , Equation (9) (b) the same product vs. α_2^{\max} , the maximum of the non-Gaussian parameter, Equation (22). The onset of the Stokes–Einstein (SE) violation for $\alpha_2^{\max} > \alpha_{2,c}^{\max}$ and $R > R_c$, respectively, is indicated with the full vertical lines (uncertainty marked by dashed lines). The thick line in the panel (a) is the master curve between $\log \tau_\alpha$ and the DW factor, Equation (A1), recast in terms of R and the thin line, is the corresponding linear approximation for small R values. Note that the SE violation is apparent where the linear approximation is poor. Data from [29].

It is seen that states with equal R (Figure 7a), i.e., states with equal DW factor according to Equation (9), exhibit nearly equal values of the product $DM\tau_\alpha$. A similar result has been reported for atomic binary mixtures [55] and metallic alloys [30]. Recognising that the diffusivity D and the structural relaxation time τ_α reflect the long time behaviour of MSD and ISF, respectively, Figure 7a reveals that Equation (3) is valid even in the *diffusive regime* which is entered in polymer melts at times fairly longer than τ_{ee} , being $\tau_{ee} \gg \tau_\alpha$.

6.2. Quasi-Universal SE Breakdown of Fragile Glass-Formers

Having noted that the SE failure is tracked by the DW factor in unentangled polymers, we now pose the question if this finding exhibits universal features. To this aim, we consider the ratio K_{SE}/K_0 with K_{SE} defined in Equation (13) and K_0 a scaling factor to ensure the unit limit value at large DW factor.

In Figure 8, we plot the ratio K_{SE}/K_0 as a function of $\langle u^2 \rangle / u_g^2$. We complement the MD results on unentangled polymers already presented in Figure 7 with other MD data, considering the diffusion of Cu and Zr atoms in metallic alloy, A and B atoms in a Lennard–Jones binary mixture [30] together with experimental data concerning the popular fragile glass-former ortho-terphenyl (OTP) [74,75]. Figure 8 evidences the good collapse of the SE violation in terms of the reduced DW.

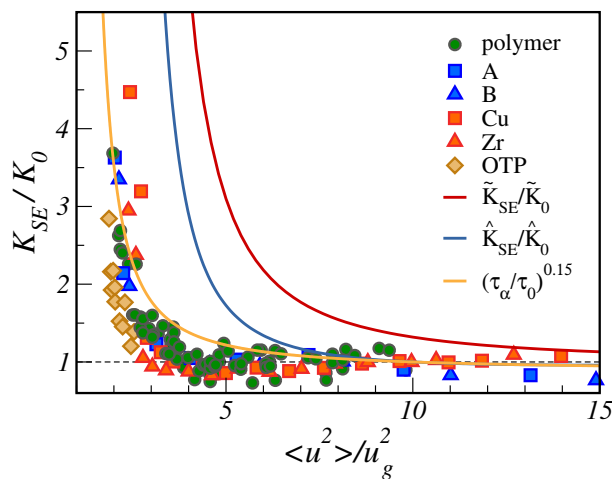


Figure 8. Stokes–Einstein product K_{SE} , normalised by its high temperature value K_0 ($\tau_\alpha \simeq 1$ ps), as a function of the reduced DW factor $\langle u^2 \rangle / u_g^2$, u_g^2 being the DW factor at the glass transition. In addition to unentangled polymers, the plot also considers MD data concerning atomic binary mixtures (atoms labelled as A and B) and metallic alloys made by Cu and Zr atoms, as well as experimental data for ortho-terphenyl (OTP) [74,75]. Two predictions of the master curve are presented in terms of the quantity \hat{K}_{SE} and \tilde{K}_{SE} , Equations (A8) and (A10), respectively. Both quantities have no adjustable parameters. \hat{K}_0 and \tilde{K}_0 are suitable constants to ensure the unit limit value at large $\langle u^2 \rangle / u_g^2$. A third master curve, drawn from the fractional SE law $\tau_\alpha^{1-\kappa}$ with $\kappa = 0.85$ (orange curve), is superimposed to the other curves. For numerical data, u_g^2 is obtained according to the procedure outlined in [47]. Data from [30].

Figure 8 offers the opportunity to test the master curve predicted by the model of Section 2 with no adjustable parameters \hat{K}_{SE} , Equation (A8), and its approximant \tilde{K}_{SE} , Equation (A10). It is seen that \hat{K}_{SE} predicts a stronger SE breakdown than actually observed. Larger deviations are exhibited by the approximant \tilde{K}_{SE} . How to improve the agreement: The expression of the diffusion coefficient in Section 2.2, assuming that displacements as large as a are statistically independent, aims at a SE product \hat{K}_{SE} , Equation (A8), with no additional adjustable parameters with respect to the ones of τ_α , i.e., the ones of Equation (A2). This puts severe constraints on the shape of the distribution of the square displacements needed to overcome the relevant energy barriers $p(a^2)$, Equation (7). The form of the distribution is adequate for large displacements to reach the transition state governing τ_α , as proven by the effective fit of the MD data by the predicted master curve shown in Figure 4. However, the findings of Figure 8 suggest that it must be improved for small displacements affecting D . Alternatively, we may also state that the distribution $p(\ln \tau)$, Equation (11), should be refined as far as the short relaxation times are concerned.

Figure 8 shows that better agreement occurs by assuming the fractional SE form $D\tau_\alpha \simeq \tau_\alpha^{1-\kappa}$ [15,31] with τ_α as given from Equation (A2). The best fit is found with $\kappa = 0.85$, which equals the universal value found by Mallamace et al. [76], deviating from the prediction of the “obstruction model” $\kappa = 2/3$ [15].

7. Displacement Correlation Length

Several results of the present paper suggest that the vibrational dynamics, as sensed by DW factor, provides insight into DH. A line of attack to understand how vibrational dynamics is related to slow relaxation is provided by the model of Section 2. The model is based on the distribution of the (squared) displacements needed by a particle to rearrange in the different local environments, Equation (7), leading in turn to the distribution of relaxation times, Equation (11). As noted in Section 6.2, the model needs further development. A further aspect to be improved is the absence of any detail on the localization of the particles with a given dynamics. This prevents any prediction concerning a peculiar aspect of DH, i.e., the existence of spatial domains with characteristic length scales where the particles undergo correlated motion, e.g., see Figure 1.

To make progress, it is worthwhile to preliminarily judge whether DW exhibits some correlation with possible dynamic length scales. To pursue this task, we studied the following monomer displacement–displacement correlation (DDC) functions [53,54]:

$$C_{\vec{u}}(r, \tau_\alpha) = \langle \hat{\mathbf{u}}_i(t_0, \tau_\alpha) \cdot \hat{\mathbf{u}}_j(t_0, \tau_\alpha) \rangle, \quad (23)$$

$$C_{\delta u}(r, \tau_\alpha) = \langle \delta u_i(t_0, \tau_\alpha) \delta u_j(t_0, \tau_\alpha) \rangle / \langle [\delta u(t_0, \tau_\alpha)]^2 \rangle. \quad (24)$$

An average over all the i -th and j -th monomers spaced by r is understood. $\hat{\mathbf{u}}_k(t_0, t)$ is the versor of the displacement vector of k -th monomer in a time interval from t_0 to $t_0 + t$, $\mathbf{u}_k(t_0, t) = \mathbf{r}_k(t_0 + t) - \mathbf{r}_k(t_0)$ and $\delta u_k(t_0, t) = |\mathbf{u}_k(t_0, t)| - \langle |\mathbf{u}(t_0, t)| \rangle$, where $|\mathbf{u}_k(t_0, t)|$ is the modulus of the displacement. Henceforth, $C_{\delta u}(r, \tau_\alpha)$ and $C_{\vec{u}}(r, \tau_\alpha)$ will be referred to as modulus (or mobility) and direction DDC functions, respectively. Local anisotropies and collective elastic solid-like response to the rattling of the monomers in the cage of their neighbours play a central role in the DDC build-up [64].

We consider DDCs of the states presented in part of the states in Figure 2. We remind that the states (i) exhibit different DH degree, e.g., see Figures 5 and 6, and (ii) are grouped in sets labelled B through E, each set being characterized by a single value of the DW factor.

Figure 9a,b shows the spatial dependence of the direction and the modulus DDC functions, respectively, for the sets of states labelled B through E in Figure 2. Both correlation functions manifest damped oscillations in-phase with the pair correlation function $g(r)$, thus evidencing that the correlated motion of a tagged monomer and its surroundings is influenced by the structure of the latter. This agrees with previous work on DDCs in Lennard–Jones systems [72,77], hard-sphere [78] and experiments on colloids [79]. The highest correlations are reached at a distance corresponding to the bond length $b = 0.97$ which demonstrates the highly concerted dynamics of bonded monomers. The correlation peaks, located at the first-, second-... neighbours shells, vanish approximately in an exponential way on increasing the distance from the tagged particle (see insets of Figure 9). In more detail, Figure 9a shows that the direction correlations do not show significant increase in their spatial extension on increasing the structural relaxation time. Figure 9b shows the modulus (mobility) correlations. Differently from the direction correlations, their spatial extension increase meaningfully with the structural relaxation time (see also the inset of Figure 9b).

Figure 9b clearly shows that physical states with equal DW factor, i.e., belonging to the same set of states (B, . . . , E), exhibit the same spatial correlations. This provides further support that Equation (3) also holds if the spatial dependence of the correlation function is considered for a given time up to τ_α at least. To provide additional insight, we evaluated the length scales of the exponential decays of the

DDC maxima with the distance $\sim \exp[-r/\xi_X(\tau_\alpha)]$ with $X = \vec{u}, \delta u$, thus defining two distinct dynamic correlation lengths pertaining to direction and modulus DDCs, $\xi_{\vec{u}}(\tau_\alpha)$ and $\xi_{\delta u}(\tau_\alpha)$, respectively. Figure 10 shows these quantities. It is seen that the spatial extension of the modulus DDC increases quite a lot with τ_α and reaches distances beyond the next-nearest neighbours for the states with the slowest relaxation. Instead, the direction correlations are virtually independent of the structural relaxation. Irrespective of the correlation length under consideration, Figure 10 also shows that they are equal within the errors for states with equal DW factor, i.e., belonging to the same set of states (B, . . . , E).

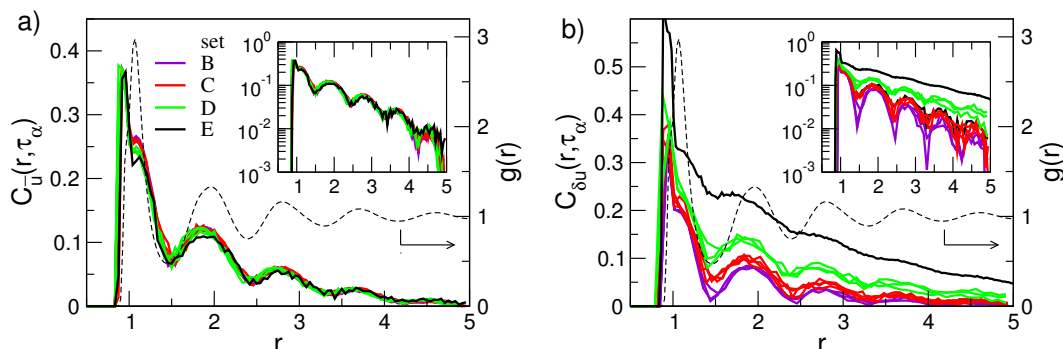


Figure 9. Radial dependence of the correlation of the direction (a) and the mobility (b) displacements occurring in a time range as wide as the structural relaxation time τ_α . For comparison, the radial distribution function $g(r)$ (dashed line) of the state with $\{M = 2, \rho = 1.086, T = 0.7, q = 7, p = 6\}$ is plotted. Note that $g(r)$ is virtually state-independent. The insets are semi-log plots of the corresponding main panels. Note the approximate exponential decay of the peak amplitudes with slopes $\xi_{\vec{u}}(\tau_\alpha)$ and $\xi_{\delta u}(\tau_\alpha)$, respectively. Data from [53].

We are now in a position to compare our results with previous work on DDCs. Simulations of Lennard–Jones binary mixture (BM) observed that at time t_α , corresponding to maximum dynamic heterogeneity, $\xi_{\delta u}^{BM}(t_\alpha)$ increases as the temperature decreases, whereas $\xi_{\vec{u}}^{BM}(t_\alpha)$ is almost constant [80]. This agrees with our findings in Figure 10 concerning unentangled polymers. As to the modulus DDC correlation length, one finds [53] that after suitable algebraic manipulation to allow comparison [79], our changes of $\xi_{\delta u}(\tau_\alpha)$ with τ_α are in quantitative agreement with the results of Bennemann et al. reported in a study of the same polymer system investigated here [72].

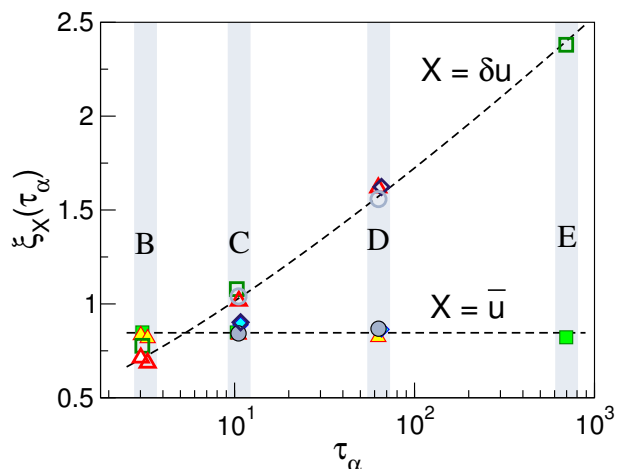


Figure 10. The direction $\xi_{\bar{u}}(\tau_\alpha)$ (full symbols) and modulus $\xi_{\delta u}(\tau_\alpha)$ (open symbols) correlation lengths vs. the structural relaxation time τ_α of selected set of states of Figure 2. Dashed lines are guides for the eyes. States with equal DW factor, i.e., belonging to the same set B, \dots , E exhibit equal directional and mobility correlation lengths. Data from [53].

8. Discussion

There is wide experimental, numerical and theoretical evidence that the fast vibrational dynamics, as sensed by the Debye–Waller factor $\langle u^2 \rangle$, and the time scale τ_α of the slow microscopic reorganisation of a liquid close to the transition to the glassy state are correlated in an universal way. Potential applicative implications concerning the quick characterisation of the stability of disordered structures with ultraslow relaxation are apparent. Less attention has been paid to a series of numerical MD simulation studies concluding in favour of strong correlations also between the vibrational dynamics and the dynamical heterogeneity, the spatial distribution of long-time mobility developing when approaching the disordered solid state. We reviewed these studies, mainly concerning melts of unentangled linear polymers, unifying all the results for the first time in terms of Equation (3). The latter has been tested both in space and time. In particular, we considered time-dependent quantities accounting for transport and relaxation like MSD, ISF and NGP and showed that they are related to the self-part of the van Hove function, which reduces to suitable correlation functions. In this respect, the correlation between the Debye–Waller factor and the breakdown of the SE law, a hallmark of DH presence, is seen as an ancillary consequence of the extension of Equation (3), which at times is much longer than τ_α , where the motion is diffusive. We also inspected Equation (3) in space by considering both the van Hove function and DDC functions. Notably, DDC functions are collective in nature, differently from the self-part of the van Hove function, which is a single-particle quantity. This suggests that Equation (3) also holds for collective correlation functions. A further validation of this conclusion is offered by the collective stress–stress correlation function, which has been presented elsewhere [32] and not discussed in this review.

The understanding of the microscopic origin of the correlation between the vibrational dynamics and the heterogeneous dynamics close to the glass transition is still unsatisfactory in several respects. In particular, both the model discussed here, as well as other ones reported in the literature, even if successful in relating the Debye–Waller factor $\langle u^2 \rangle$ with the time scale τ_α , are currently unable to account for the fact evidenced by the numerical simulations that the vibrational dynamics conveys also information on the spatial correlations between the mobility of different particles.

9. Methods

Most results discussed in this review concern a coarse-grained model of a linear polymer chain with M monomers is adopted. Bending and torsional potentials are neglected, i.e., the chain is fully flexible. While addressing the interested reader to the referenced papers for further details, we provide here some general aspect of the numerical model. We considered systems with total number of monomer $N \geq 2000$. Non-bonded monomers at a distance r interact via the truncated parametric potential:

$$U_{q,p}(r) = \frac{\epsilon}{p-q} \left[p \left(\frac{\sigma^*}{r} \right)^q - q \left(\frac{\sigma^*}{r} \right)^p \right] + U_{cut} \quad (25)$$

where $\sigma^* = 2^{1/6}\sigma$ and the value of the constant U_{cut} are chosen to ensure $U_{p,q}(r) = 0$ at $r \geq r_c = 2.5\sigma$. The minimum of the potential $U_{p,q}(r)$ is at $r = \sigma^*$, with a constant depth $U(r = \sigma^*) = \epsilon$. Note that $U_{q,p}(r) = U_{p,q}(r)$. Bonded monomers interact with a potential which is the sum of the Finitely Extendible Nonlinear Elastic (FENE) potential and the Lennard–Jones (LJ) potential [71]. The resulting bond length is $b = 0.97\sigma$, within a few percent. We set $\sigma = 1$ and $\epsilon = 1$. The time unit is $\tau_{MD} = (m\sigma^2/\epsilon)^{1/2}$, with m being the mass of the monomer. Temperature is in units of ϵ/k_B , where k_B is the Boltzmann constant. We set $m = k_B = 1$. All the data presented in this work are expressed in reduced MD units. It is interesting to map the reduced MD units to real physical units. The procedure involves the comparison of the experiment with simulations and provide the basic length (σ), temperature (ϵ/k_B) and time (τ_{MD}) units [69,71,81–83]. For polyethylene and polystyrene, it was found $\sigma = 5.3 \text{ \AA}$, $\epsilon/k_B = 443 \text{ K}$, $\tau_{MD} = 1.8 \text{ ps}$ and $\sigma = 9.7 \text{ \AA}$, $\epsilon/k_B = 490 \text{ K}$, $\tau_{MD} = 9 \text{ ps}$, respectively [69]. For poly(vinyl alcohol) $\sigma = 5.2 \text{ \AA}$, $\epsilon/k_B = 550 \text{ K}$ and $\tau_{MD} = 1.63 \text{ ps}$ [83]. For polyisoprene $\sigma = 6.7 \text{ \AA}$, $\epsilon/k_B = 307 \text{ K}$ and $\tau_{MD} = 10 \text{ ps}$ [81]. The densities used in this and other studies are lower than the densities at atmospheric pressure, e.g., when mapping our model to polyethylene and polystyrene, one finds ~ 0.5 and $\sim 0.7 \text{ g/cm}^3$, to be compared to the actual values 0.78 and 0.92 g/cm^3 , respectively [69].

Author Contributions: F.P., A.T. and D.L. wrote the manuscript together. All authors have read and approved the final version.

Funding: This research was funded by the project PRA- 2018-34 (“ANISE”) from the University of Pisa.

Acknowledgments: A generous grant of computing time from IT Center, University of Pisa, and Dell EMC® Italia is gratefully acknowledged.

Conflicts of Interest: The authors declare no conflicts of interest.

Abbreviations

The following abbreviations are used in this manuscript.

DDC	displacement–displacement correlation
DH	dynamical heterogeneity
DW	Debye–Waller
ISF	Intermediate scattering function
MD	Molecular-dynamics
MSD	Mean square displacement
NGP	non-Gaussian parameter
SE	Stokes–Einstein

Appendix A

Appendix A.1. Structural Relaxation

According to the model detailed in Section 2.1, the master curve relating the structural relaxation time τ_α and the DW factor $\langle u^2 \rangle$, Equation (2), takes the form given by Equation (8). Other variants of Equation (8) are of interest in the comparison with numerical and experimental results. As an example, the best fit of the master curve Equation (8) with the numerical data concerning the melt of unentangled polymer chains of interest here yields (in MD units) [47,48]:

$$\log \tau_\alpha = \alpha + \beta \frac{1}{\langle u^2 \rangle} + \gamma \frac{1}{\langle u^2 \rangle^2} \quad (\text{A1})$$

where $\alpha = -0.424(1)$, $\beta = \bar{a}^2 / (2 \ln 10) = 2.7(1) \cdot 10^{-2}$, $\gamma = \sigma_{a^2}^2 / (8 \ln 10) = 3.41(3) \cdot 10^{-3}$.

To recast Equation (A1) as a universal master curve removing system-dependent quantities, one considers the DW factor at the glass transition u_g^2 (defined via $\tau_\alpha = 10^2$ s) and introduces the reduced variable $\langle u^2 \rangle / \langle u_g^2 \rangle$, so as to write Equation (A1),

$$\ln \tau_\alpha = \hat{\alpha} + \hat{\beta} \frac{\langle u_g^2 \rangle}{\langle u^2 \rangle} + \hat{\gamma} \left(\frac{\langle u_g^2 \rangle}{\langle u^2 \rangle} \right)^2 \quad (\text{A2})$$

where $\hat{\alpha} = 2 \ln 10 - \hat{\beta} - \hat{\gamma}$. The ansatz is that Equation (A2) is system-independent and both $\hat{\beta}$ and $\hat{\gamma}$ are universal coefficients. To derive their numerical values, we use the value $\langle u_g^2 \rangle^{1/2} = 0.129$ and the best-fit values of α, β, γ , drawn from the numerical simulations of the melt of unentangled polymer chains [47,48]. This yields $\hat{\beta} = 3.7(1)$ and $\hat{\gamma} = 28.4(2)$ [30].

Appendix A.2. Diffusion Coefficient

The diffusion coefficient is evaluated from Equation (12) via Equations (4) and (7). The result is

$$D(\langle u^2 \rangle) = \frac{\sigma_{a^2}}{6\tau_0} \exp \left[-\frac{1}{2} \left(\frac{\bar{a}^2}{\sigma_{a^2}} \right)^2 \right] \frac{G(\langle u^2 \rangle)}{\sqrt{18\pi} \left[1 + \operatorname{erf}(\bar{a}^2 / \sqrt{2}\sigma_{a^2}) \right]} \quad (\text{A3})$$

where

$$\begin{cases} G(x) = \{1 - \sqrt{\pi} \Lambda_-(x) \exp[\Lambda_-^2(x)] \operatorname{erfc}[\Lambda_-(x)]\} \\ \Lambda_\pm(x) = \frac{\sigma_{a^2}^2 \pm 2\bar{a}^2 x}{\sqrt{8}\sigma_{a^2} x} \end{cases} \quad (\text{A4})$$

As $\tau_\alpha^{(HW)}(a^2)$ depends on the parameter a in a much more marked way than a^2 , see Equation (4), an effective approximation of the diffusivity, as expressed by Equation (12), is $D \simeq \tilde{D}$ with

$$\tilde{D} = \frac{a_0^2}{6} \left\langle 1/\tau_\alpha^{(HW)}(a^2) \right\rangle_{a^2} \quad (\text{A5})$$

where a_0 is a constant.

Appendix A.3. Stokes–Einstein Product

After suitable manipulation the Stokes–Einstein product K_{SE} , Equation (13), takes the form ($M = 1$)

$$K_{SE}(\langle u^2 \rangle) = D(\langle u^2 \rangle) \times \tau_\alpha(\langle u^2 \rangle) \quad (\text{A6})$$

where

$$\begin{cases} K_{SE}(x) = \sigma_{a^2} F(x) G(x) \\ F(x) = \frac{1}{\sqrt{18\pi}} \exp[\Lambda_+^2(x)] \exp\left[-\left(\frac{\bar{a}^2}{\sigma_{a^2}}\right)^2\right] \frac{1+\text{erf}(\Lambda_+[x])}{[1+\text{erf}(\bar{a}^2/\sqrt{2\sigma_{a^2}})]^2} \end{cases} \quad (\text{A7})$$

where the auxiliary functions $G(x)$ and $\Lambda_\pm(x)$ are defined in Appendix A.2.

When expressed in terms of the adimensional quantity $z = \langle u^2 \rangle / u_g^2$, the product K_{SE} takes the form $\hat{K}_{SE}(z)$ with

$$\begin{cases} \hat{K}_{SE}(z) = u_g^2 \hat{F}(z) \{1 - \sqrt{\pi} \hat{\Lambda}_-(z) \exp[\hat{\Lambda}_-^2(z)] \text{erfc}[\hat{\Lambda}_-(z)]\} \\ \hat{\Lambda}_\pm(z) = \frac{2\hat{\gamma} \pm \hat{\beta} z}{2\hat{\gamma}^{1/2} z} \\ \hat{F}(z) = \frac{2}{3} \sqrt{\frac{\hat{\gamma}}{\pi}} \exp[\hat{\Lambda}_+^2(z)] \exp\left[-\frac{\hat{\beta}^2}{2\hat{\gamma}}\right] \frac{1+\text{erf}(\hat{\Lambda}_+[z])}{[1+\text{erf}(\hat{\beta}/2\hat{\gamma}^{1/2})]^2} \end{cases} \quad (\text{A8})$$

The quantities $\hat{\beta}$ and $\hat{\gamma}$ are defined in Appendix A.1.

The Stokes–Einstein product K_{SE} may be approximated as $K_{SE} \simeq \tilde{K}_{SE}$ with $\tilde{K}_{SE} = \tilde{D}\tau_\alpha$, where \tilde{D} is defined in Appendix A.2. This yields

$$\tilde{K}_{SE} = \frac{a_0^2}{6} \left\langle \tau_\alpha^{(HW)}(a^2) \right\rangle_{a^2} \left\langle 1/\tau_\alpha^{(HW)}(a^2) \right\rangle_{a^2} \quad (\text{A9})$$

The explicit expression of the quantity \tilde{K}_{SE} , in terms of $z = \langle u^2 \rangle / u_g^2$, reads

$$\tilde{K}_{SE}(z) = \frac{a_0^2}{6} \exp\left[2\hat{\gamma}/z^2\right] \frac{\left[1 + \text{erf}\left(\frac{\hat{\gamma}^{1/2}}{z} + \frac{\hat{\beta}}{2\hat{\gamma}^{1/2}}\right)\right] \left[\text{erfc}\left(\frac{\hat{\gamma}^{1/2}}{z} - \frac{\hat{\beta}}{2\hat{\gamma}^{1/2}}\right)\right]}{\left[1 + \text{erf}\left(\frac{\hat{\beta}}{2\hat{\gamma}^{1/2}}\right)\right]^2} \quad (\text{A10})$$

Appendix B

The van Hove function for a uniform fluid is defined as

$$G(\mathbf{r}, t) = \frac{1}{N} \left\langle \sum_{i=1}^N \sum_{j=1}^N \delta[\mathbf{r} + \mathbf{x}_i(0) - \mathbf{x}_j(t)] \right\rangle \quad (\text{A11})$$

Physically, $Gd\mathbf{r}$ is the probability of finding a particle j in a region $d\mathbf{r}$ around a point \mathbf{r} at time t if the particle i was at the origin at time 0. We may recast the van Hove function by resorting to the time-dependent, microscopic particle density [26]

$$\rho(\mathbf{r}, t) = \sum_{i=1}^N \delta[\mathbf{r} - \mathbf{x}_i(t)] \quad (\text{A12})$$

We rewrite Equation (A11) as

$$G(\mathbf{r}, t) = \frac{1}{N} \left\langle \int \sum_{i=1}^N \sum_{j=1}^N \delta[\mathbf{r}' + \mathbf{r} - \mathbf{x}_j(t)] \delta[\mathbf{r}' - \mathbf{x}_i(0)] d\mathbf{r}' \right\rangle \quad (\text{A13})$$

$$= \frac{1}{N} \int \langle \rho(\mathbf{r}' + \mathbf{r}, t) \rho(\mathbf{r}', 0) d\mathbf{r}' \rangle \quad (\text{A14})$$

$$= \frac{1}{\rho} \langle \rho(\mathbf{r}, t) \rho(\mathbf{0}, 0) \rangle \quad (\text{A15})$$

where ρ is the average number density. Equation (A15) shows that the van Hove function is proportional to the density correlation function. It is easily shown that the van Hove function may be written as [26]

$$G(\mathbf{r}, t) = G_s(\mathbf{r}, t) + G_d(\mathbf{r}, t) \quad (\text{A16})$$

where $G_s(\mathbf{r}, t)$ and $G_d(\mathbf{r}, t)$ are usually called the “self” and “distinct” parts. Equation (18) provides the explicit expression of $G_s(\mathbf{r}, t)$. The distinct part is written as

$$G_d(\mathbf{r}, t) = \frac{1}{N} \left\langle \sum_{i=1}^N \sum_{j \neq i}^N \delta[\mathbf{r} + \mathbf{x}_i(0) - \mathbf{x}_j(t)] \right\rangle \quad (\text{A17})$$

Finally, we show that both $G_s(\mathbf{r}, t)$ and $G_d(\mathbf{r}, t)$ may be expressed in terms of suitable correlation functions. To this aim, we define the auxiliary function $B^i(\mathbf{r}, t) \equiv \delta[\mathbf{r} - \mathbf{x}_i(t)]$. By repeating the same passages leading from Equation (A11) to Equation (A13), one has

$$G_s(\mathbf{r}, t) = \frac{1}{N} \left\langle \int \sum_{i=1}^N \delta[\mathbf{r}' + \mathbf{r} - \mathbf{x}_i(t)] \delta[\mathbf{r}' - \mathbf{x}_i(0)] d\mathbf{r}' \right\rangle \quad (\text{A18})$$

$$= \frac{1}{N} \int \sum_{i=1}^N \langle B^i(\mathbf{r}' + \mathbf{r}, t) B^i(\mathbf{r}', 0) d\mathbf{r}' \rangle \quad (\text{A19})$$

$$= \frac{1}{\rho} \sum_{i=1}^N \langle B^i(\mathbf{r}, t) B^i(\mathbf{0}, 0) \rangle \quad (\text{A20})$$

The last passage follows from the uniformity of the fluid. Analogously, one finds

$$G_d(\mathbf{r}, t) = \frac{1}{\rho} \sum_{i=1}^N \sum_{j \neq i}^N \langle B^i(\mathbf{r}, t) B^j(\mathbf{0}, 0) \rangle \quad (\text{A21})$$

References

1. Angell, C. Relaxation in liquids, polymers and plastic crystals-strong/fragile patterns and problems. *J. Non-Cryst. Sol.* **1991**, 131–133, 13–31.
2. Debenedetti, P.G.; Stillinger, F.H. Supercooled liquids and the glass transition. *Nature* **2001**, 410, 259–267.
3. Ngai, K.L. *Relaxation and Diffusion in Complex Systems*; Springer: Berlin, Germany, 2011.
4. Sillescu, H. Heterogeneity at the glass transition: A review. *J. Non-Cryst. Solids* **1999**, 243, 81–108.
5. Ngai, K.L. Why the fast relaxation in the picosecond to nanosecond time range can sense the glass transition. *Philos. Mag.* **2004**, 84, 1341–1353.
6. Berthier, L.; Biroli, G. Theoretical perspective on the glass transition and amorphous materials. *Rev. Mod. Phys.* **2011**, 83, 587–645.
7. Ashcroft, N.W.; Mermin, N.D. *Solid State Physics*; Holt, Rinehart and Wiston: New York, NY, USA, 1976.

8. Simmons, D.S.; Cicerone, M.T.; Zhong, Q.; Tyagic, M.; Douglas, J.F. Generalized localization model of relaxation in glass-forming liquids. *Soft Matter* **2012**, *8*, 11455–11461.
9. Pazmiño Betancourt, B.A.; Hanakata, P.Z.; Starr, F.W.; Douglas, J.F. Quantitative relations between cooperative motion, emergent elasticity, and free volume in model glass-forming polymer materials. *Proc. Natl. Acad. Sci. USA* **2015**, *112*, 2966–2971.
10. Douglas, J.F.; Pazmiño Betancourt, B.A.; Tong, X.; Zhang, H. Localization model description of diffusion and structural relaxation in glass-forming Cu–Zr alloys. *J. Stat. Mech. Theory Exp.* **2016**, *2016*, 054048.
11. Ediger, M.D. Spatially heterogeneous dynamics in supercooled liquids. *Annu. Rev. Phys. Chem.* **2000**, *51*, 99–128.
12. Richert, R. Heterogeneous dynamics in liquids: Fluctuations in space and time. *J. Phys. Condens. Matter* **2002**, *14*, R703–R738.
13. Tarjus, G.; Kivelson, D. Breakdown of the Stokes–Einstein relation in supercooled liquids. *J. Chem. Phys.* **1995**, *103*, 3071–3073.
14. Tracht, U.; Wilhelm, M.; Heuer, A.; Feng, H.; Schmidt-Rohr, K.; Spiess, H.W. Length Scale of Dynamic Heterogeneities at the Glass Transition Determined by Multidimensional Nuclear Magnetic Resonance. *Phys. Rev. Lett.* **1998**, *81*, 2727–2730.
15. Douglas, J.; Loporini, D. Obstruction model of the fractional Stokes–Einstein relation in glass-forming liquids. *J. Non-Cryst. Solids* **1998**, *235–237*, 137–141.
16. Jung, Y.; Garrahan, J.P.; Chandler, D. Excitation lines and the breakdown of Stokes–Einstein relations in supercooled liquids. *Phys. Rev. E* **2004**, *69*, 061205.
17. Adam, G.; Gibbs, J.H. On the Temperature Dependence of Cooperative Relaxation Properties in Glass-Forming Liquids. *J. Chem. Phys.* **1965**, *43*, 139–146.
18. Starr, F.W.; Douglas, J.F.; Sastry, S. The relationship of dynamical heterogeneity to the Adam-Gibbs and random first-order transition theories of glass formation. *J. Chem. Phys.* **2013**, *138*, 12A541, doi:10.1063/1.4790138.
19. Karmakar, S.; Dasgupta, C.; Sastry, S. Length scales in glass-forming liquids and related systems: A review. *Rep. Prog. Phys.* **2015**, *79*, 016601.
20. Albert, S.; Bauer, T.; Michl, M.; Biroli, G.; Bouchaud, J.P.; Loidl, A.; Lunkenheimer, P.; Tourbot, R.; Wiertel-Gasquet, C.; Ladieu, F. Fifth-order susceptibility unveils growth of thermodynamic amorphous order in glass-formers. *Science* **2016**, *352*, 1308–1311.
21. Biroli, G.; Karmakar, S.; Procaccia, I. Comparison of Static Length Scales Characterizing the Glass Transition. *Phys. Rev. Lett.* **2013**, *111*, 165701.
22. Wyart, M.; Cates, M.E. Does a Growing Static Length Scale Control the Glass Transition? *Phys. Rev. Lett.* **2017**, *119*, 195501.
23. Androzzzi, L.; Schino, A.D.; Giordano, M.; Loporini, D. Evidence of a fractional DebyeStokesEinstein law in supercooled oterphenyl. *Europhys. Lett.* **1997**, *38*, 669–674.
24. De Michele, C.; Loporini, D. Viscous flow and jump dynamics in molecular supercooled liquids. II. Rotations. *Phys. Rev. E* **2001**, *63*, 036702.
25. Tyrrell, H.J.V.; Harris, K.R. *Diffusion in Liquids*; Butterworths: London, UK, 1984.
26. Hansen, J.P.; McDonald, I.R. *Theory of Simple Liquids*, 3rd ed.; Academic Press: New York, NY, USA, 2006.
27. De Michele, C.; Loporini, D. Viscous flow and jump dynamics in molecular supercooled liquids. I. Translations. *Phys. Rev. E* **2001**, *63*, 036701.
28. Lad, K.N.; Jakse, N.; Pasturel, A. Signatures of fragile-to-strong transition in a binary metallic glass-forming liquid. *J. Chem. Phys.* **2012**, *136*, 104509.
29. Puosi, F.; Loporini, D. Communication: Fast and local predictors of the violation of the Stokes- Einstein law in polymers and supercooled liquids. *J. Chem. Phys.* **2012**, *136*, 211101.
30. Puosi, F.; Loporini, D. Communication: Fast dynamics perspective on the breakdown of the Stokes–Einstein law in fragile glass-formers. *J. Chem. Phys.* **2018**, *148*, 131102.
31. Chang, I.; Fujara, F.; Geil, B.; Heuberger, G.; Mangel, T.; Sillescu, H. Translational and rotational molecular motion in supercooled liquids studied by NMR and forced Rayleigh scattering. *J. Non-Cryst. Solids* **1994**, *172–175*, 248–255.

32. Puosi, F.; Leporini, D. Communication: Correlation of the instantaneous and the intermediate-time elasticity with the structural relaxation in glass-forming systems. *J. Chem. Phys.* **2012**, *136*, 041104.
33. Tobolsky, A.; Powell, R.E.; Eyring, H. Elastic-viscous properties of matter. In *Frontiers in Chemistry*; Burk, R.E.; Grummit, O., Eds.; Interscience: New York, NY, USA, 1943; Volume 1, pp. 125–190.
34. Hall, R.W.; Wolynes, P.G. The aperiodic crystal picture and free energy barriers in glasses. *J. Chem. Phys.* **1987**, *86*, 2943–2948.
35. Angell, C.A. Formation of glasses from liquids and biopolymers. *Science* **1995**, *267*, 1924–1935.
36. Dyre, J.C.; Olsen, N.B.; Christensen, T. Local elastic expansion model for viscous-flow activation energies of glass-forming molecular liquids. *Phys. Rev. B* **1996**, *53*, 2171–2174.
37. Martinez, L.M.; Angell, C.A. A thermodynamic connection to the fragility of glass-forming liquids. *Nature* **2001**, *410*, 663–667.
38. Sastry, S. The relationship between fragility, configurational entropy and the potential energy landscape of glass-forming liquids. *Nature* **2001**, *409*, 164–167.
39. Ngai, K.L. Dynamic and thermodynamic properties of glass-forming substances. *J. Non-Cryst. Solids* **2000**, *275*, 7–51.
40. Xia, X.; Wolynes, P.G. Fragilities of liquids predicted from the random first order transition theory of glasses. *Proc. Natl. Acad. Sci. USA* **2000**, *97*, 2990–2994.
41. Buchenau, U.; Zorn, R. A relation between fast and slow motions in glassy and liquid selenium. *Europhys. Lett.* **1992**, *18*, 523–528.
42. Starr, F.; Sastry, S.; Douglas, J.F.; Glotzer, S. What do we learn from the local geometry of glass-forming liquids? *Phys. Rev. Lett.* **2002**, *89*, 125501.
43. Bordat, P.; Affouard, F.; Descamps, M.; Ngai, K.L. Does the interaction potential determine both the fragility of a liquid and the vibrational properties of its glassy state? *Phys. Rev. Lett.* **2004**, *93*, 105502.
44. Widmer-Cooper, A.; Harrowell, P. Predicting the Long-Time Dynamic Heterogeneity in a Supercooled Liquid on the Basis of Short-Time Heterogeneities. *Phys. Rev. Lett.* **2006**, *96*, 185701.
45. Zhang, H.; Srolovitz, D.J.; Douglas, J.F.; Warren, J.A. Grain boundaries exhibit the dynamics of glass-forming liquids. *Proc. Natl. Acad. Sci. USA* **2009**, *106*, 7735–7740.
46. Widmer-Cooper, A.; Perry, H.; Harrowell, P.; Reichman, D.R. Irreversible reorganization in a supercooled liquid originates from localized soft modes. *Nat. Phys.* **2008**, *4*, 711–715.
47. Larini, L.; Ottochian, A.; De Michele, C.; Leporini, D. Universal scaling between structural relaxation and vibrational dynamics in glass-forming liquids and polymers. *Nat. Phys.* **2008**, *4*, 42–45.
48. Ottochian, A.; De Michele, C.; Leporini, D. Universal divergenceless scaling between structural relaxation and caged dynamics in glass-forming systems. *J. Chem. Phys.* **2009**, *131*, 224517.
49. Puosi, F.; Leporini, D. Scaling between Relaxation, Transport, and Caged Dynamics in Polymers: From Cage Restructuring to Diffusion. *J. Phys. Chem. B* **2011**, *115*, 14046–14051.
50. Ottochian, A.; Leporini, D. Scaling between structural relaxation and caged dynamics in $Ca_{0.4}K_{0.6}(NO_3)_{1.4}$ and glycerol: Free volume, time scales and implications for the pressure-energy correlations. *Philos. Mag.* **2011**, *91*, 1786–1795.
51. Ottochian, A.; Leporini, D. Universal scaling between structural relaxation and caged dynamics in glass-forming systems: Free volume and time scales. *J. Non-Cryst. Solids* **2011**, *357*, 298–301.
52. De Michele, C.; Del Gado, E.; Leporini, D. Scaling between Structural Relaxation and Particle Caging in a Model Colloidal Gel. *Soft Matter* **2011**, *7*, 4025–4031.
53. Puosi, F.; Leporini, D. Spatial displacement correlations in polymeric systems. *J. Chem. Phys.* **2012**, *136*, 164901.
54. Puosi, F.; Leporini, D. Erratum: “Spatial displacement correlations in polymeric systems” [*J. Chem. Phys.* *136*, 164901 (2012)]. *J. Chem. Phys.* **2013**, *139*, 029901.
55. Puosi, F.; Michele, C.D.; Leporini, D. Scaling between relaxation, transport and caged dynamics in a binary mixture on a per-component basis. *J. Chem. Phys.* **2013**, *138*, 12A532.
56. Ottochian, A.; Puosi, F.; Michele, C.D.; Leporini, D. Comment on “Generalized localization model of relaxation in glass-forming liquids”. *Soft Matter* **2013**, *9*, 7890–7891.

57. Novikov, V.N.; Sokolov, A.P. Role of Quantum Effects in the Glass Transition. *Phys. Rev. Lett.* **2013**, *110*, 065701.
58. Puosi, F.; Chulkin, O.; Bernini, S.; Capaccioli, S.; Leporini, D. Thermodynamic scaling of vibrational dynamics and relaxation. *J. Chem. Phys.* **2016**, *145*, 234904.
59. Guillaud, E.; Joly, L.; de Ligny, D.; Merabia, S. Assessment of elastic models in supercooled water: A molecular dynamics study with the TIP4P/2005f force field. *J. Chem. Phys.* **2017**, *147*, 014504.
60. Horstmann, R.; Vogel, M. Common behaviours associated with the glass transitions of water-like models. *J. Chem. Phys.* **2017**, *147*, 034505.
61. Becchi, M.; Giuntoli, A.; Leporini, D. Molecular layers in thin supported films exhibit the same scaling as the bulk between slow relaxation and vibrational dynamics. *Soft Matter* **2018**, *14*, 8814–8820.
62. Bernini, S.; Puosi, F.; Leporini, D. Thermodynamic scaling of relaxation: Insights from anharmonic elasticity. *J. Phys. Condens. Matter* **2017**, *29*, 135101.
63. Puosi, F.; Leporini, D. The kinetic fragility of liquids as manifestation of the elastic softening. *Eur. Phys. J. E* **2015**, *38*, 87.
64. Bernini, S.; Leporini, D. Cage effect in supercooled molecular liquids: Local anisotropies and collective solid-like response. *J. Chem. Phys.* **2016**, *144*, 144505.
65. Allen, M.P.; Tildesley, D.J. *Computer Simulations of Liquids*; Oxford University Press: New York, NY, USA, 1987.
66. Doi, M.; Edwards, S.F. *The Theory of Polymer Dynamics*; Clarendon Press: Oxford, UK, 1988.
67. Boon, J.P.; Yip, S. *Molecular Hydrodynamics*; Dover Publications: New York, NY, USA, 1980.
68. Gedde, U.W. *Polymer Physics*; Chapman and Hall: London, UK, 1995.
69. Kröger, M. Simple models for complex nonequilibrium fluids. *Phys. Rep.* **2004**, *390*, 453–551.
70. Kob, W.; Donati, C.; Plimpton, S.J.; Poole, P.H.; Glotzer, S.C. Dynamical Heterogeneities in a Supercooled Lennard–Jones Liquid. *Phys. Rev. Lett.* **1997**, *79*, 2827–2830.
71. Baschnagel, J.; Varnik, F. Computer simulations of supercooled polymer melts in the bulk and in confined geometry. *J. Phys. Condens. Matter* **2005**, *17*, R851–R953.
72. Bennemann, C.; Donati, C.; Baschnagel, J.; Glotzer, S.C. Growing range of correlated motion in a polymer melt on cooling towards the glass transition. *Nature* **1999**, *399*, 246–249.
73. Ottochian, A.; De Michele, C.; Leporini, D. Non-Gaussian effects in the cage dynamics of polymers. *Philos. Mag.* **2008**, *88*, 4057–4062.
74. Tölle, A. Neutron scattering studies of the model glass former ortho -terphenyl. *Rep. Prog. Phys.* **2001**, *64*, 1473.
75. Chang, I.; Sillescu, H. Heterogeneity at the Glass Transition: Translational and Rotational Self-Diffusion. *J. Phys. Chem. B* **1997**, *101*, 8794–8801.
76. Mallamace, F.; Branca, C.; Corsaro, C.; Leone, N.; Spooren, J.; Chen, S.H.; Stanley, H.E. Transport properties of glass-forming liquids suggest that dynamic crossover temperature is as important as the glass transition temperature. *Proc. Natl. Acad. Sci. USA* **2010**, *107*, 22457–22462.
77. Donati, C.; Glotzer, S.C.; Poole, P.H. Growing Spatial Correlations of Particle Displacements in a Simulated Liquid on Cooling toward the Glass Transition. *Phys. Rev. Lett.* **1999**, *82*, 5064–5067, doi:10.1103/PhysRevLett.82.5064.
78. Doliwa, B.; Heuer, A. Cooperativity and spatial correlations near the glass transition: Computer simulation results for hard spheres and disks. *Phys. Rev. E* **2000**, *61*, 6898–6908.
79. Weeks, E.R.; Crocker, J.C.; Weitz, D.A. Short and long-range correlated motion observed in colloidal glasses and liquids. *J. Phys. Condens. Matter* **2007**, *19*, 205131.
80. Narumi, T.; Tokuyama, M. Simulation study of spatial, Atemporal correlation functions in supercooled liquids. *Philos. Mag.* **2008**, *88*, 4169–4175.
81. Kremer, K.; Grest, G.S. Dynamics of entangled linear polymer melts: A molecular-dynamics simulation. *J. Chem. Phys.* **1990**, *92*, 5057–5086.
82. Paul, W.; Smith, G.D. Structure and dynamics of amorphous polymers: Computer simulations compared to experiment and theory. *Rep. Prog. Phys.* **2004**, *67*, 1117–1185.
83. Luo, C.; Sommer, J.U. Coding coarse grained polymer model for LAMMPS and its application to polymer crystallization. *Comput. Phys. Commun.* **2009**, *180*, 1382–1391.